

LIMNOLOGY and OCEANOGRAPHY



© 2020 The Authors. *Limnology and Oceanography* published by Wiley Periodicals LLC on behalf of Association for the Sciences of Limnology and Oceanography. doi: 10.1002/lno.11542

Flow-induced reconfiguration of aquatic plants, including the impact of leaf sheltering

Xiaoxia Zhang , 1,2* Heidi Nepf1

¹Department of Civil and Environmental Engineering, Massachusetts Institute of Technology, Cambridge, Massachusetts ²State Key Laboratory of Hydraulics and Mountain River Engineering, Sichuan University, Chengdu, Sichuan, China

Abstract

Many aquatic plants are flexible and bend in response to current. This reconfiguration can reduce the drag on the plant, both by reducing the frontal area and by creating a more streamlined shape. Previous studies have considered how the buoyancy and rigidity of a plant impact the drag reduction. This study additionally considered how reconfiguration impacts the sheltering between leaves on a plant and how this, in turn, impacts the drag on the plant. The posture and drag of single-stemmed, leaved plants were studied through a combination of laboratory experiments and theoretical modeling using both plastic *Rotala bonsai* and live *Bacopa caroliniana*. The laboratory experiments measured drag and posture on individual plants over a range of channel velocity. The theoretical model calculated plant posture and drag based on a force balance that included buoyancy, the restoring force due to stem stiffness, and leaf drag modified to account for sheltering between leaves. Leaf sheltering was characterized by a sheltering coefficient, C_s , which is a function of the plant posture, leaf angle, leaf spacing, and leaf width. C_s decreased from 1 to a minimum value, C_{s0} , associated with a fully deflected, horizontal stem posture. Once validated, the model was used to explore a range of leaf configurations, following examples found in real plants. The modeling and experiments revealed conditions for which drag increased with reconfiguration, and also that the drag reached a finite, limiting value for horizontal stem posture. Neither trend has been described in previous reconfiguration models.

Aquatic plants are common features in many environments, including rivers, flood plains, coastal regions, and shallow lakes. They provide many ecosystem services, such as producing and storing carbon (Greiner et al. 2013; Tang et al. 2018), enhancing bed and embankment stability (Barbier et al. 2011; Arkema et al. 2017), and providing shelter (Costanza et al. 1997) and food (Waycott et al. 2005) for fish and aquatic invertebrates. Aquatic plants can be adversely impacted by hydrodynamic drag forces which can damage (Duan et al. 2006) or uproot (Schutten et al. 2005) them. Flexible plants can diminish their exposure to drag by bending in response to flow, which is called reconfiguration (e.g., Vogel 1989; Sand-Jensen 2003). The reconfiguration of a plant depends on its stiffness and material density. Natural plants exhibit a wide range of behavior, from highly flexible seagrass, which bends easily in weak current, to reeds and trees, whose greater stiffness limit bending, except in very high current.

This is an open access article under the terms of the Creative Commons Attribution License, which permits use, distribution and reproduction in any medium, provided the original work is properly cited.

Additional Supporting Information may be found in the online version of this article.

The change in drag due to reconfiguration has been quantified by a dimensionless parameter called the Vogel number, ν_r defined within the context of the power law dependence of the drag force, F, with the velocity, $F \sim U^{2+\nu}$ (e.g., Vogel 1984; Gosselin et al. 2010; de Langre et al. 2012). A negative Vogel number indicates that the drag dependence on velocity is weaker than quadratic, i.e., drag is reduced relative to a rigid body. Harder et al. (2004) summarized the Vogel number measured for different plant species, which ranged from $\nu = -1.3$ to -0.1, including marine (e.g., Carrington 1990; Friedland and Denny 1995 freshwater (e.g., Usherwood et al. 1997; Schutten and Davy 2000), and terrestrial vegetation (e.g., Vogel 1989; Gillies et al. 2002; Harder et al. 2004). In addition to varying between species, the Vogel number can also vary with flow velocity for a single plant. For example, Harder et al. (2004; Figure 4b) estimated the Vogel number for the giant reed, Arundo donax, and found $\nu = -0.12$ for wind speeds between 0 and 1 m/s and $\nu = -0.71$ for wind speed above 1.5 m/s. Further, the presence and number of leaves can alter the plantscale Vogel number. For example, the Vogel number of twigs with leaves was observed to be -1 to -0.4 (Figure 4 in Västilä and Järvelä 2014), which was lager in magnitude than the Vogel number of the stem alone (-0.32 to -0.2), suggesting that the reconfiguration of leaves played a dominant role in the reduction of plant-scale drag. In addition, Västilä and

^{*}Correspondence: xiaoxia@mit.edu

Järvelä (2014) observed that the force per leaf area decreased as the number of leaves increased (increasing leaf area to stem area), suggesting that leaf sheltering was also contributing to the reduction in plant-scale drag. The contribution of leaf sheltering to drag reduction has not been explicitly included in models predicting the impact of reconfiguration on drag. The goal of this paper was to consider this mechanism.

Many previous studies have examined the drag force on leaves and its contribution to the total drag on a branch or tree. For example, individual broad leaves, especially those with long petioles and bilaterally lobed or heart-shaped bases, reconfigure into cones under strong wind (10-20 m/s), which significantly reduces their drag (Vogel 1989). Leaves can contribute 10-90% of the total drag on trees and individual branches (based on flume tests reported in Xavier et al. 2010; Jalonen and Järvelä 2013; Whittaker et al. 2013; Västilä and Järvelä 2014). Because of leaf reconfiguration, the fraction of leaf drag decreases with increasing velocity. For example, Figure 6 in Jalonen and Järvelä (2013) shows that leaves contribute up to 80% of the total drag on a tree dragged through water at low speed (0.1 m/s), but only 40% when the speed exceeded 0.8 m/s. Whittaker et al. (2013) observed that the drag contribution from leaves varied with species, with foliage contributing 75% of the total drag on Alnus glutinosa, but only 30% of the total drag on Salix alba. In contrast to tree species with significant leaf reconfiguration, the present study considered submerged plant species for which the leaves exhibit little reconfiguration, even as stem reconfiguration changes the overall plant posture. In this case drag reduction is not associated with leaf reconfiguration, but instead with the activation of leaf sheltering as the plant reconfigures.

Several previous studies have developed scaling laws predicting the Vogel exponent for simple structures such as beams, rods, and plates, and an excellent review of these models is provided in Gosselin (2019). For example, at sufficiently high velocity, flat plates, filaments (Gosselin et al. 2010; Gosselin and De Langre 2011), and rod-shaped fibers (Alben et al. 2002 exhibit 2-D reconfiguration, which produces a Vogel number $\nu = -2/3$. 3-D reconfiguration, such as the rolling up of tuliptree leaf (Vogel 1989) or a Iridaea flaccida blade (Gaylord et al. 1994), has been studied by Schouveiler and Boudaoud (2006) using a disk cut along its radius, such that the disk rolls up into an increasingly acute cone as the flow speed increases. This 3-D reconfiguration produces a Vogel number $\nu = -4/3$. Luhar and Nepf (2011) expanded the 2-D reconfiguration model of Gosselin et al. (2010) by including buoyancy. The influence of drag, buoyancy, and elastic restoring force on a simple 2-D structure (e.g., flat blade or cylindrical stem) can be characterized by two dimensionless parameters, the Buoyancy number B (representing the ratio of restoring force due to buoyancy and restoring force due to stiffness) and the Cauchy number (representing the relative magnitude of hydrodynamic drag and the restoring force due to stiffness). The existing definition of Cauchy number will be denoted as Ca^* (Eq. 2), so that we can later introduce a modified Cauchy number (*Ca*) specific to the more complex morphology considered in this study.

$$B = \frac{\Delta \rho g V_p l^2}{EI} \tag{1}$$

$$Ca^* = \frac{1}{2} \frac{\rho C_D b U^2 l^3}{EI}$$
 (2)

Here, $\Delta \rho$ is the density difference between water (ρ) and plant (ρ_p) . g is the gravitational acceleration. V_p is the total volume of the plant, which equals btl or $\pi D^2 l/4$ for a flat blade or cylindrical stem, respectively, with b, t, D, and l the width, thickness, diameter, and length, respectively. E is the elastic modulus, and I is the second momnt of area. For a flat blade, $I = bt^3/12$. For a cylindrical stem, $I = \pi D^4/64$. C_D is the drag coefficient. U is the velocity.

To describe the reduction in drag associated with blade reconfiguration, Luhar and Nepf (2011) introduced the effective blade length, l_e , defined as the length of a rigid, vertical blade that generates the same drag as a flexible blade with length l. The effective length is related to the Vogel number, $l_e/l\sim U^{\nu}$ (see discussion in Pan et al. 2014). Using theory and simulation, Luhar and Nepf (2011) derived the functional dependence of l_e on Ca^* and B. When buoyancy is negligible, $l_e/l\sim U^{-2/3}\sim Ca^{*-1/3}$, consistent with 2-D bending ($\nu=-2/3$, e.g., Gosselin 2019). Luhar and Nepf (2013) predicted the flow within and above a submerged meadow of flexible blades using this drag model for a single blade, demonstrating that a physical description of an individual plant can be extended to predict flow-vegetation interaction at the canopy scale.

The model proposed by Luhar and Nepf (2011) assumes a blade morphology, representing the seagrass Zostera marina (Fig. 1) and the freshwater grass Vallisneria natans. For a simple blade morphology, in which the bending element is the same as the drag generating element, $l_e/l\sim Ca^{*-1/3}$ ($\nu=-2/3$, e.g., Alben et al. 2002; Gosselin et al. 2010; Luhar and Nepf 2011). Plants with a rod geometry, such as Equisetum hymale (Horsetail rush) also follows the 2-D bending model, with $l_e/l\sim Ca^{*-1/3}$ $(\nu = -2/3, \text{ Hassani et al. 2016})$. Other aquatic grasses are composed of a slender stem with multiple leaves. The leaves have many shapes: needle, feathery, round, short, and long. In addition, the leaves may attach to the stem directly (e.g., Elodea nuttallii) or be linked through thin stalks called petioles (e.g., Ludwigia repens). When multiple leaves are attached to a stem by petioles, both the stem and petioles may reconfigure, which approximates a 3-D reconfiguration. Consistent with this, Puijalon et al. (2005) measured the drag on Mentha aquatica, which has leaves attached by petioles, and found a Vogel number of $\nu = -1.2$ to -0.75, which is higher than the 2-D reconfiguration value ($\nu = -2/3$) and approaching the value of 3-D reconfiguration ($\nu = -4/3$). When leaves are attached to the stem directly (without petioles), the leaves are less prone to reconfiguration. This is particularly true when the leaf is short

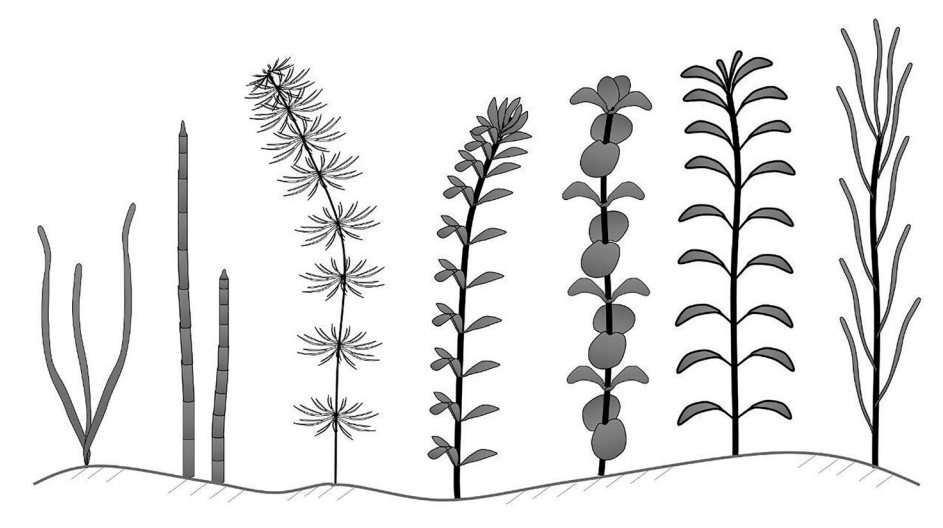


Fig. 1. Schematic of common aquatic grasses. From left to right: Zostera marina, Equisetum hymale, Ceratophyllum demersum, Elodea nuttallii, Rotala bonsai, Ludwigia repens, and Potamogeton illinoensis.

and wraps around the stem (e.g., *Rotala bonsai* in Fig. 1), forcing the leaf to arch, which makes it more resistant to bending. In this case, the stem reconfigures to a much greater degree than the leaves, which has been observed for *R. bonsai* and *Bacopa caroliniana* (as discussed in this paper). For this morphology, the leaves provide most of the drag, while the stem does most of the bending. With this disconnection between the drag and bending elements, a new model must be developed to predict the plant posture and drag. Further, for plants with many leaves distributed along the stem (Fig. 1), as the stem bends the upstream leaves may shelter downstream leaves, providing additional drag reduction. This paper uses laboratory experiments with plastic and live plants to guide the extension of previous models (e.g., Gosselin et al. 2010; Luhar and Nepf 2011) to plants with leaves, specifically accounting for the sheltering between leaves.

Theoretical model to predict drag and posture of buoyant, flexible vegetation with multiple leaves

A model to describe the reconfiguration and drag for a plant with evenly distributed leaves (Fig. 2), such as R. bonsai (Fig. 1) and B. caroliniana, was developed with the following assumptions. (1) The material density of the stem and leaves is uniform and constant (ρ_p). (2) The leaves are distributed uniformly along the stem and each leaf has the same size (length l_l , width l_w , and area A_l). (3) The leaves do not deform and the angle between the leaf and stem (α) remains unchanged as the stem bends. (4) The stem diameter (D) and elastic modulus E are constant. (5) The lift force is assumed to be negligible. Finally, (6) the drag associated with the leaves is much larger than the drag associated with the stem, such that the drag on the stem is neglected.

A curved coordinate system is used to describe the stem reconfiguration (Fig. 2). The coordinate along the stem is s, with s = 0 at the base and s = l at the top of stem, l is the

height of the plant when fully erect. θ is the local angle between the stem and vertical. For simplicity, the forces exerted on the leaves are assumed to be distributed uniformly along the stem, such that the buoyancy force (f_B) per stem length is:

$$f_B = \frac{\Delta \rho g V_p}{l} = \frac{\left(\rho - \rho_p\right) g V_p}{l} \tag{3}$$

For a rigid plant, the total drag force can be expressed as:

$$F_r = \frac{1}{2}\rho C_D A_r U^2 \tag{4}$$

in which A_r is the total projected area of a rigid plant onto the vertical. The subscript r denotes the conditions for the rigid, erect plant. The velocity (U) is assumed to be steady and uniform over depth. Since the drag on the stem was neglected, A_r

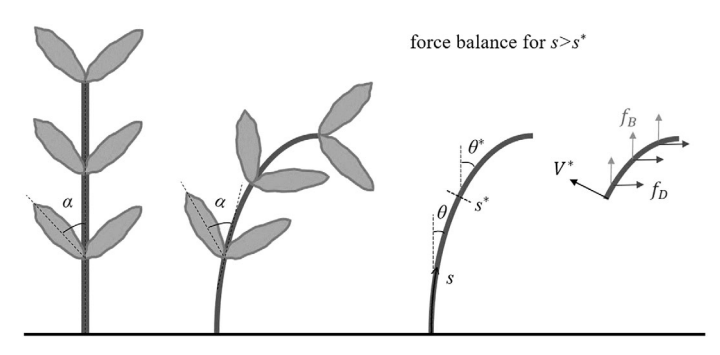


Fig. 2. Schematic of model plant with evenly distributed leaves, such as *Rotala bonsai* and *Bacopa caroliniana*. In these species, the leaves attach directly to the stem, such that the angle between the stem and leaf (α) remains the same, even as the stem reconfigures. The coordinate system along the stem, s, is zero at the base and s = l at the top of the stem.

is the sum of projected area of each leaf, $A_r = NA_l |cos\alpha|$, with A_l the area of a single leaf and N the number of leaves. For simplicity, the leaves are assumed to emerge in pairs and to be distributed equally at the left and right side of the stem (see Fig. 2). When the plant is deflected, the stem has angle θ to vertical, changing the angle between the leaves and vertical to $|\theta - \alpha|$ and $|\theta + \alpha|$ for the leaves on the upstream (left) and downstream (right) sides of the stem, respectively. Consequently, the drag force per stem length, f_D , is a function of θ and varies along the stem. Finally, for some stem angles, upstream leaves may shelter downstream leaves, reducing the drag on downstream leaves. To account for this, a sheltering coefficient, C_s , is included in the model. The form drag per stem length can then be described as the sum of drag on the upstream leaves and downstream leaves (first and second term in the numerator, respectively):

$$f_D = \frac{1}{2}\rho C_D C_s \frac{\left(\frac{N}{2}A_l|cos(\theta - \alpha)| + \frac{N}{2}A_l|cos(\theta + \alpha)|\right)}{l}U^2$$
 (5)

Since $A_r = NA_l |cos\alpha|$, f_D can be expressed in terms of A_r ,

$$f_D = \frac{1}{2}\rho C_D C_S \frac{A_r \left| \cos(\theta - \alpha) \right| + \left| \cos(\theta + \alpha) \right|}{l} U^2 \tag{6}$$

Note that Eq. 6 neglects skin friction and stem drag, because the leaf form drag dominates for most leaf orientation. An exception occurs for an initially vertical plant with horizontal leaves ($\alpha = 90^{\circ}$, $\theta = 0$), for which Eq. 6 predicts zero drag, such that the model plant will not reconfigure, which is unrealistic.

When the stem reconfigures, a stem-normal restoring force (V) is generated, with magnitude equal to the derivative of internal bending moment $(M = EI(\frac{d\theta}{ds}))$, i.e.,

$$V = -EI\frac{d^2\theta}{ds^2} \tag{7}$$

The stem-normal force balance for stem section $s > s^*$, where s^* is an arbitrary position along the stem, can be expressed as:

$$-EI\frac{d^{2}\theta}{ds^{2}}|s^{*} + \Delta\rho g V_{p}/l(l-s^{*})sin\theta^{*}$$

$$= \frac{1}{2}\rho C_{D}\frac{A_{r}}{l}U^{2}\int_{s^{*}}^{l}C_{s}\frac{|cos(\theta-\alpha)| + |cos(\theta+\alpha)|}{2|cos\alpha|}cos\theta^{*}ds$$
(8)

In dimensionless form, Eq. 8 is:

$$-\frac{d^{2}\theta}{ds^{2}}|\hat{s}^{*} + B(l - \hat{s}^{*})sin\theta^{*} = Ca\int_{\hat{s}^{*}}^{l} C_{s} \frac{|cos(\theta - \alpha)| + |cos(\theta + \alpha)|}{2|cos\alpha|}cos\theta^{*}d\hat{s}$$
(9)

in which $\hat{s} = s/l$, B was defined in Eq. 1, but the Cauchy number, Ca, has been modified to reflect the more complex plant geometry considered here. Specifically,

$$Ca = \frac{\frac{1}{2}\rho C_D A_r U^2}{EI/l^2} = \frac{\text{drag on leaves in rigid upright posture}}{\text{restoring force in stem}}$$
 (10)

This modified Cauchy number reflects the fact that the drag is associated with the projected area of the leaves, A_r , and the rigidity is associated with the stem, represented by stem length scale l. Finally, two boundary conditions are needed to use Eq. 9 to predict the plant posture and drag. As in previous studies (e.g., Alben et al. 2002), the following two boundary conditions were applied: $\theta = 0$ at $\hat{s} = 0$ and $d\theta/d\hat{s} = 0$ at $\hat{s} = 1$. The total drag on the deflected plant, F_e , can be then obtained by integrating f_D (Eq. 6) along the stem.

$$F_{e} = \int_{0}^{l} f_{D} ds = \int_{0}^{l} \frac{1}{2} \rho C_{D} C_{s} \frac{A_{r} |cos(\theta - \alpha)| + |cos(\theta + \alpha)|}{2|cos\alpha|} U^{2} ds = \frac{1}{2} \rho C_{D} A_{e} U^{2}$$
(11)

The right-most expression defines an effective area, A_e . Similar to the effective length (l_e) defined in Luhar and Nepf (2011), A_e is the area of rigid plant that provides the same drag as a flexible plant. With this definition, the ratio of drag on a flexible plant to the drag on a rigid plant can be represented as a ratio of areas, specifically, A_e/A_r (Eq. 12).

$$F_e/F_r = A_e/A_r = \int_0^l C_s \frac{|\cos(\theta - \alpha)| + |\cos(\theta + \alpha)|}{2|\cos\alpha|} ds$$
 (12)

These ratios are linked to the Vogel number which was defined within the context of quadratic dependence of the drag force, F_e , with the velocity, i.e., $F_e \sim U^{2+\nu}$ (Vogel 1984). For a rigid plant $F_r \sim U^2$, such that $F_e/F_r = A_e/A_r \sim U^\nu$ (see more discussion in Pan et al. 2014).

The sheltering coefficient, C_s , describes the drag reduction associated with the sheltering between leaves. The sheltering of elements within an array has been studied in both air (e.g., Wang and Takle 1997; Bitsuamlak et al. 2010; Wu et al. 2010) and water (Barsu et al. 2016; Jin et al. 2018). Based on these studies, C_s is expected to depend on the leaf width (l_w) and spacing (d), the angle between leaf and stem (α), and the angle of the stem to vertical (θ) . For simplicity, consider a linear stem that tilts relative to the vertical (Fig. 3). For a linear stem, the angle θ is related to the ratio of deflected height, h, and stem length, l, specifically, $cos\theta = h/l$. As the stem tilts, sheltering between leaves will occur when two conditions are met. First, part of the upstream leaf must be in-line with the downstream leaf. Second, the spacing ratio (d/l_w) must be small enough that the downstream leaf falls within the wake of the upstream leaf. These two conditions are discussed in more detail below.

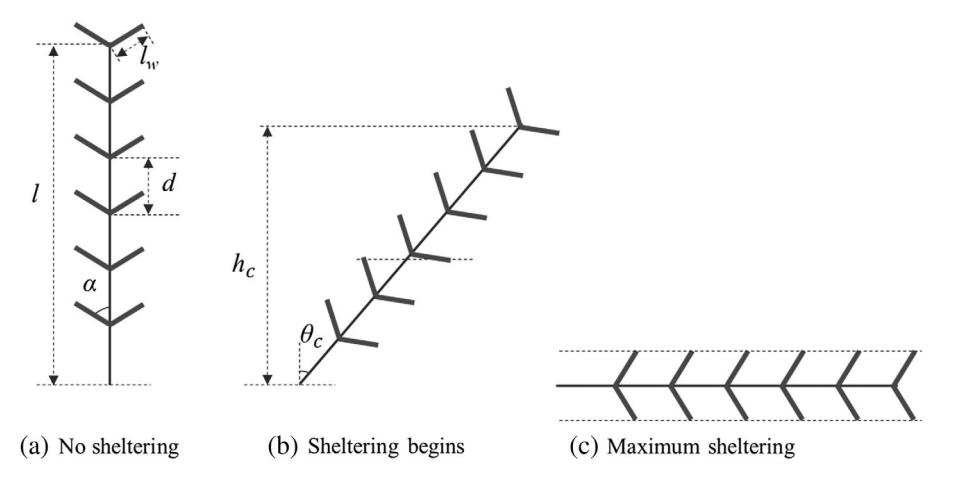


Fig. 3. Illustration of leaf sheltering that arises from plant reconfiguration. (**a**) Vertical plant posture with no sheltering. (**b**) The critical posture at which the sheltering begins, denoted by critical angle, θ_c and critical deflected height, h_c . (**c**) The final posture (horizontal) at which maximum sheltering occurs, i.e., the minimum value of the sheltering coefficient, C_{s0} .

First, sheltering can only occur if part of an upstream leaf falls in front of a downstream leaf. Consider the plant illustrated in Fig. 3, as the plant deflects from its vertical position, at some degree of deflection the top of the upstream leaf will just pass the plane of the downstream leaf. This position will be denoted as the critical deflected height, h_c , illustrated in Fig. 3b. The critical posture can also be described by the critical tilting angle θ_c , which is geometrically related to the critical deflected height, i.e., $cos\theta_c = h_c/l$. The critical angle, θ_c , is defined by geometry, as expressed in Eq. 13.

$$\delta_1 l_1 |\cos(\theta_c - \alpha)| + \delta_2 l_1 |\cos(\theta_c + \alpha)| - d|\cos\theta_c| = 0$$
 (13)

in which $\delta_1=0$ when $\theta_c-\alpha<-\pi/2$ (may occur when $\alpha>\pi/2$), other wise, $\delta_1=1$. Similarly, $\delta_2=0$ when $\theta_c+\alpha<\pi/2$, other wise, $\delta_2=1$. Note that values of θ range from 0 to $\pi/2$ and α range from 0 to π . The sheltering coefficient $C_s=1$ when $\theta<\theta_c$, i.e., $h>h_c$. C_s decreases as θ increases from θ_c to $\pi/2$ (h decreasing from h_c to 0) at which point the plant reaches the maximum reconfiguration with a horizontal posture (Fig. 3c). At this posture, the sheltering coefficient reaches a minimum value, defined as C_{s0} .

Second, the degree of sheltering in the final horizontal posture will depend mainly on leaf spacing (d) and leaf width (l_w) , the smaller dimension of the leaf). Results from Barsu et al. (2016) provide insight into the dependence of sheltering on leaf spacing and leaf width. Specifically, Barsu et al. (2016) measured the drag on a row of blades considering different blade width and different spacing between blades. In comparison to the drag measured for an isolated blade, they showed that the drag is reduced due to sheltering when the spacing, d, is less than four times l_w . Further, Figure 6b in Barsu et al. (2016) shows that the drag coefficient decreases linearly with decreasing leaf spacing for $d_c < 4l_w$. Based on this, we assume that the critical spacing for sheltering to occur is $d_c = 4l_w$, and for $d \ge d_c$, $C_{s0} = 1$. The critical value $d_c = 4l_w$

makes sense because the recirculation zone developed behind an isolated flat plate is approximately 4 time the plate width (Barsu et al. 2016). For $d < d_c$, Figure 6b in Barsu et al. (2016) suggests the following linear relationship.

$$C_{s0} = d/(4l_w) \tag{14}$$

Combining the above considerations and assuming C_s decreases linearly with deflected plant height, h/l, we have:

$$C_{s} = \begin{cases} 1 & d \ge d_{c} \text{ or } h \ge h_{c} \\ \frac{1 - C_{s0} h}{h_{c} / l} + C_{s0} & d < d_{c} \text{ and } h < h_{c} \end{cases}$$
(15)

Laboratory experiments were conducted to first verify Eq. 14. Next, measured values of plant posture and drag were used to verify the prediction of plant posture and drag using Eq. 9 and Eq. 12, which incorporated the sheltering coefficient (Eq. 15). Because C_s and h/l are mutually dependent, the following iterative method was needed to predict drag and plant posture. An initial sheltering coefficient $C_{s1} = 1$ was applied to Eq. 9 to calculate h_1/l . Next, C_{s2} was calculated from h_1/l and Eq. 15. After this, C_{s2} was applied to Eq. 9 to calculate h_2/l . This was repeated until step i, for which the difference between h_i/l and h_{i-1}/l was less than 1%.

Laboratory experiments

Three types of experiments were conducted using plastic and live plants. First, in Experiment 1, the limiting sheltering coefficient C_{s0} (Eq. 14), was studied using plastic R. bonsai leaves distributed along a thin rigid wire (with 0.9 mm diameter), held rigidly by a small post at stem angle $\theta = 90^{\circ}$ representing the most extreme stem reconfiguration (Fig. 4a). The number of leaf pairs was varied from 1 to 20, and the spacing between leaves ranged from infinite to 0.5 cm. Two types of

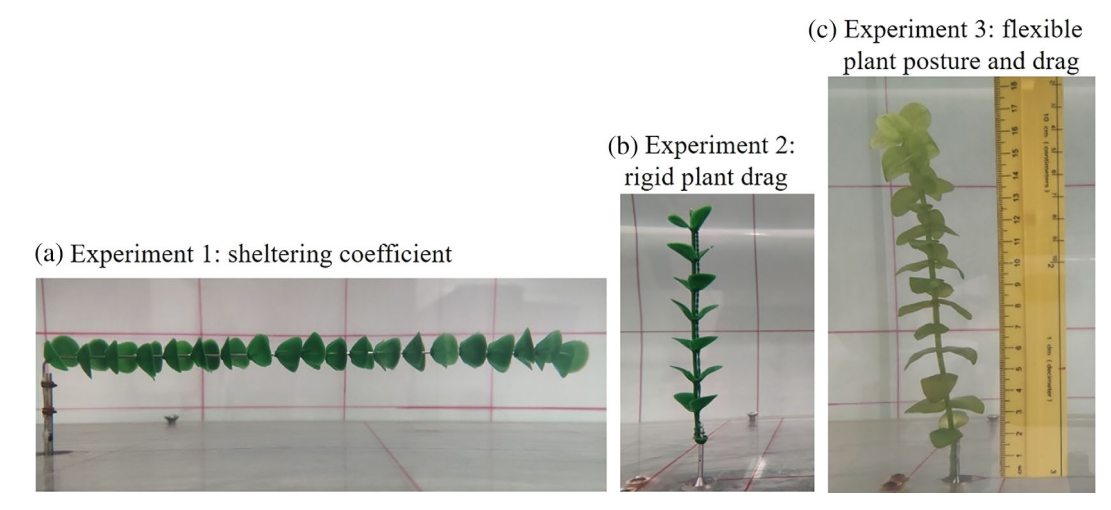


Fig. 4. Photos from experiments: (a) an array of leaves used to quantify the limiting sheltering coefficient, C_{s0} . (b) Rigid plastic *Rotala bonsai* used to establish the baseline drag force for a rigid plastic plant. (c) Live *Bacopa caroliniana* used to validate the model prediction of plant posture and plant drag force

leaf distributions were tested, type 1: pairs of leaves aligned along the stem, as assumed in the theoretic model (*see* Fig. 4a) and type 2: pairs of leaves alternating by 90° rotation along the wire, representative of many real plants (e.g., Fig. 4c). The drag force on 1 leaf and on N leaves were F_{D1} and F_{DN} , respectively. In each case, the drag force on the wire and post alone was measured and subtracted. Assuming all leaves have equal area, $C_{s0} = F_{DN}/(NF_{D1})$.

Second, in Experiment 2, rigid model plants were used to establish the baseline drag on a rigid plant without reconfiguration (Fig. 4b). The stem was made rigid by attaching a thin steel wire (1 mm diameter) along the back of the stem. To simplify the analysis, Eq. 4 was rewritten as $F_r = kU^2$, with $k = \frac{1}{2}\rho C_D A_r$. The coefficient k was estimated for a 10-cm plant exposed to velocity U = 5-26 cm/s (Fig. 4b). For a rigid vertical plant with uniformly distributed leaves, the total drag is proportional to stem length, such that the value of k measured for the 10-cm plant could be used to estimate the drag on a longer rigid plant. Specifically, $F_r = nkU^2$, in which n=1, 2, 3, and 4 for plants with length l=10, 20, 30, and 40 cm, respectively. Applying, $F_r = nkU^2$ to Eq. 10, the Cauchy number becomes,

$$Ca = \frac{nkU^2l^2}{EI} \tag{16}$$

For the live B. caroliniana, there was no way to attach a rigid steel support without breaking the leaves. As an alternate method, the forces measured for the shortest B. caroliniana at the lowest three velocities (1.75–7.2 cm/s) were used to define the coefficient k and Ca. For this plant and over these three velocities the drag varied quadratically with velocity.

Third, in Experiment 3, flexible model *R. bonsai* (plastic plant, $\rho_p=914$ kg/m³, $E=1.11\times10^8$ Pa, $I=3.79\times10^{-13}$ m⁴)

and live B. caroliniana (ρ_p =748 kg/m³, E = 7.51 × 10⁶ Pa, $I = 2.02 \times 10^{-12} \text{ m}^4$) were used to validate the prediction of plant posture and drag over a range of velocity. For example, Fig. 4c shows a live specimen of B. caroliniana. To capture a wide range of Cauchy number, four different lengths of plastic R. bonsai (10, 20, 30, and 40 cm) and three different lengths of live B. caroliniana (9, 17, and 28 cm) were studied (Table 1). The stem rigidity, EI, was measured with the cantilever beam method using a 5-cm stem specimen (leaves removed). Based on five replicate tests on the plastic sample the uncertainty was 2%. With the velocity U = 2-62 cm/s, the Cauchy number ranged from Ca = 0.01-3000. The uncertainty in the drag force was estimated to be 10% based on repeated measurements in Experiment 2. Along with the uncertainty of 1% in stem length and 2% in stem rigidity EI, the uncertainty of Cauchy number was approximately 10%.

All the experiments were conducted in a 24-m-long, 38-cm-wide, 60-cm-depth recirculating flume. Velocity was adjusted using two variable speed pumps. To reduce wave generation at the inflow, two layers of rubberized coconut fiber (80 cm length, 38 cm width, 10 cm thickness) were placed just below the water surface at the channel inlet (*see* Fig. 5).

In each experiment, a single live or model plant was attached to a 2.5-cm tall stainless steel post with 2-mm diameter, which was connected to a submersible force sensor (Futek LSB210 100 g, see Fig. 5). The sensor was calibrated by National Instrument (NI-USB 9237), and force measurements were logged to a computer using a data acquisition module (Lei and Nepf 2019). The force measurements had an accuracy of 10%. The force sensor was mounted beneath an acrylic ramp (1-m top length, 2-m bottom length, 13-cm height, and spanning the flume width) to avoid interaction between flow and the sensor. For each flow condition, the drag force was measured for 3 min at a sampling rate of 1600 Hz.

Table 1. List of experiment tested cases. h_c/l was estimated by $\cos\theta_c = h_c/l$ and θ_c was calculated by Eq. 13. With the uncertainty of leaf angle being \pm 5°, the uncertainty of h_c/l was 2%. C_{s0} was estimated using Eq. 14 with an uncertainty of 10%. B was calculated by Eq. 1 with an estimated uncertainty of 5%.

Plant	<i>EI</i> (10 ⁻⁵ Nm ²)	α	h _c /I	C_{s0}	<i>l</i> (cm)	В
Rotala bonsai	4.22	48°	0.91	0.25	10, 20, 30, 40	0.4, 1.8, 5.9, 14
Bacopa caroliniana	1.51	112°	0.99	0.125	9, 17, 28	1.4, 8.6, 37

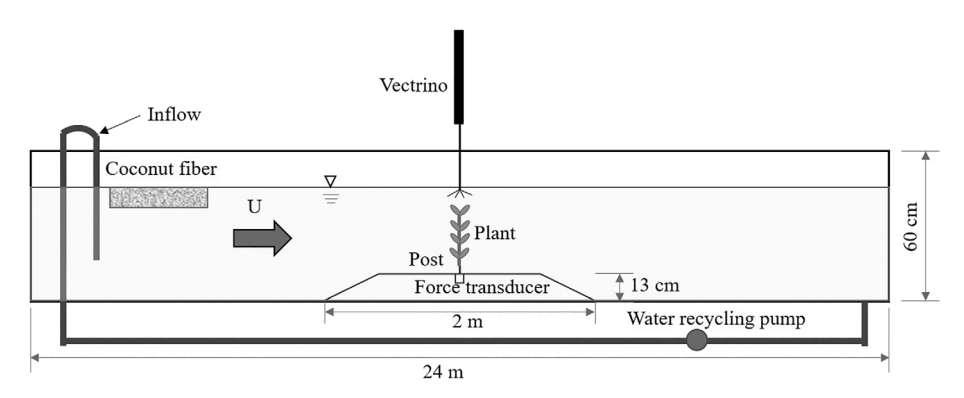


Fig. 5. Schematic of the experimental setup. Velocity was adjusted with a variable speed pump. A post connected the plant to the force sensor and elevated the plant above the boundary layer. The force sensor was housed inside an acrylic ramp that was 13-cm high and 2-m long. Velocity profiles were recorded with a Nortek Vectrino at the place where the plant was mounted, but after the plant, post, and force sensor were removed.

Experiments with plastic plants were repeated four times while live plants were tested one time to keep the plants in good condition. A separate force measurement was made on the post alone (without plant) at each velocity, and the force on the post was subtracted from the force measured with the plant and post together. During each force measurement, digital images were captured by a smart cellphone (MIX 2S) camera with 12 million pixels in each photo. The camera was fixed to a tripod by a self-stick holder. The camera captured 100 photos in 10 s. This sampling frequency (10 Hz) was much higher than the estimated 0.1-0.8 Hz stem natural frequency (Table 8.1 in Blevins 1979) and 0.2-1 Hz vortex shedding frequency from the plant leaves (e.g., Blevins 1990), and the 10-s duration included a minimum of 10 cycles of possible oscillation. Twenty photos spaced 0.5 s apart were selected from each burst to obtain the range of plant posture and the deflected plant height. A photo with a ruler beside the plant (Fig. 4c) was used to calculate the scale (pixels/cm).

Three water depths, 16, 22, and 32 cm (above the ramp) were selected to achieve the desired velocity and maintain complete submergence of the plant. The Froude number ranged from 0.01 to 0.5. After the force measurements, the plant, post, and force sensor were removed, and an acoustic Doppler velocimeter (ADV, Nortek Vectrino) was used to measure velocity profiles at the middle of the ramp where the plant had been located. The vertical resolution of the velocity profile was 1 cm to 3 cm. At each measurement point, the Vectrino recorded a 3-min record with a sampling frequency

of 200 Hz. The post elevated the plant above the boundary layer on the ramp, so that the plant experienced a nearly uniform velocity over depth (see Figure 3 in Luhar and Nepf 2011). Each velocity measurement was quality checked by the signal to noise ratio and de-spiked with the following method. First, the acceleration thresholding method identified and removed spikes in the velocity time series if the instantaneous acceleration was higher than the acceleration of gravity g (Nikora and Goring 2000). Second, the time-mean velocity \bar{u} and standard deviation σ of the remaining data were calculated and the velocity component u_i was removed if $|u_i - \bar{u}| > 3\sigma$ (Goring and Nikora 2002). Finally, the depth-averaged velocity \bar{u} between 3 cm above ramp and flow surface.

Results

Sheltering coefficient

In Experiment 1 (Fig. 4a), force measurements made on a horizontal stem with leaves of varied spacing (d) were used to estimate the limiting sheltering coefficient, C_{s0} , representing the condition with maximum sheltering. The measured values of C_{s0} are plotted as a function of the ratio of spacing (d) to leaf width (l_w) in Fig. 6. There was no systematic difference between the cases with aligned leaves (type 1) and alternating leaves (type 2), indicating the theoretic model assumption of aligned leaves was reasonable. At the maximum spacing ($d/l_w = 7.5$), $C_{s0} = 1$, indicating that no sheltering impacted

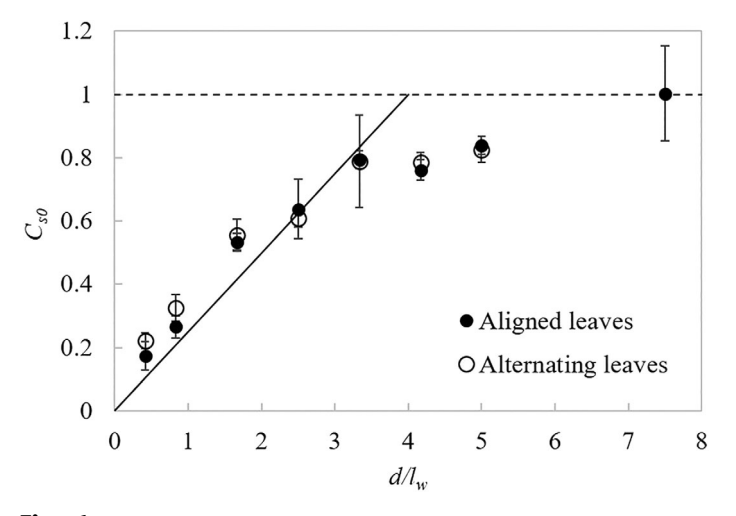


Fig. 6. The sheltering coefficient associated with maximum sheltering, C_{s0} , estimated from a plant with horizontal posture (Fig. 4a) as a function of the ratio of leaf spacing (*d*) to leaf width (I_w). The dots and circles are the mean values of four repeated measurements with type 1 leaf configuration (pairs of leaves aligned along the stem) and type 2 leaf configuration (pairs of leaves alternating by 90° rotation along the stem), respectively. The error bars are the standard deviation of four repeated measurements. The horizontal dashed line indicates no sheltering and the solid line indicates a sheltering relation of $C_{s0} = d/(4I_w)$.

the drag on individual leaves. For spacing less than $d/l_w = 5$, the sheltering coefficient decreased (indicating increasing sheltering) as d/l_w decreased. This trend agreed with the observations in Barsu et al. (2016), despite the different shape in model leaves. Specifically, they noted that C_{s0} decreased linearly from 1 for $d/l_w < 4$, as shown with a solid black line in Fig. 6, corresponding to $C_{s0} = d/(4l_w)$, i.e., Eq. 14. Note that for $d/l_w \le 2$, $C_{s0} = d/(4l_w)$ underestimated C_{s0} , i.e., overestimated the sheltering effect because the first leaf will never be sheltered, such that the drag cannot actually reach zero. The same underestimation of C_{s0} by Eq. 14 (overestimation of sheltering) would also occur for a small number (< 4) of leaves, because the drag on the first leaf, which is never sheltered, would be a large fraction of the total leaf drag.

Drag force on rigid plant

As expected, the drag force measured for the rigid plastic plant, F_r , followed a quadratic dependence on velocity (e.g., Fig. 7). The slope of F_r vs. U^2 was denoted as $k = 1/2\rho C_D A_r$. For the 10-cm long rigid plant, $k = 0.488 \pm 0.009 \text{ Nm}^{-2} \text{ s}^2$ (Fig. 7a). The smallest specimen (l = 9 cm) of live B. caroliniana exhibited limited reconfiguration at the three lowest velocity conditions, such that the drag increased linearly with velocity squared (Fig. 7b), providing an estimation of the rigid drag factor, $k = 0.97 \pm 0.02 \text{ Nm}^{-2} \text{ s}^2$ (Fig. 7b).

Reconfiguration of and drag on flexible model plant with leaves

This section describes the measured deflected stem height and drag force and makes comparison to the model prediction. Consistent with the model assumption, the leaves in the experiment did not deform, even as the stem was deflected horizontally (see images in Fig. 8). The drag reduction was framed in terms of the effective area ratio, defined as the ratio of effective frontal area to rigid frontal area, A_e/A_r , which was estimated from the ratio of drag force on a flexible plant F_e to drag force on a rigid upright plant F_n as defined in Eq. 12. Figure 8 shows the measured and modeled values of stem deflected height, h/l, and effective area ratio, A_e/A_r , for the plastic model of R. bonsai (with $l_w = 1.2$ cm, d = 1.2 cm, $\alpha = 48^{\circ}$, and from Eq. 14 $C_{s0} = 0.25$). The critical posture was $\theta_c = 24^{\circ}$ ($h_c/l = 0.91$) as calculated from Eq. 13. See the summary of parameters in Table 1. To capture the range of Buoyancy number (B = 0.4-14), model predictions were made for B = 0 and 20. Images of plant posture at different Cauchy numbers are included at the bottom of Fig. 8. Note that the plant was not perfectly straight, and image 1 represents the fully erect posture, which was the same as that observed for zero current. The red lines in the plant images are the postures predicted from the model (Eq. 9). The model captured the trends in both deflected height (h/l) and effective area ratio (A_e/A_r) over the entire Cauchy number range. The maximum error between the modeled and measured values of h/l and

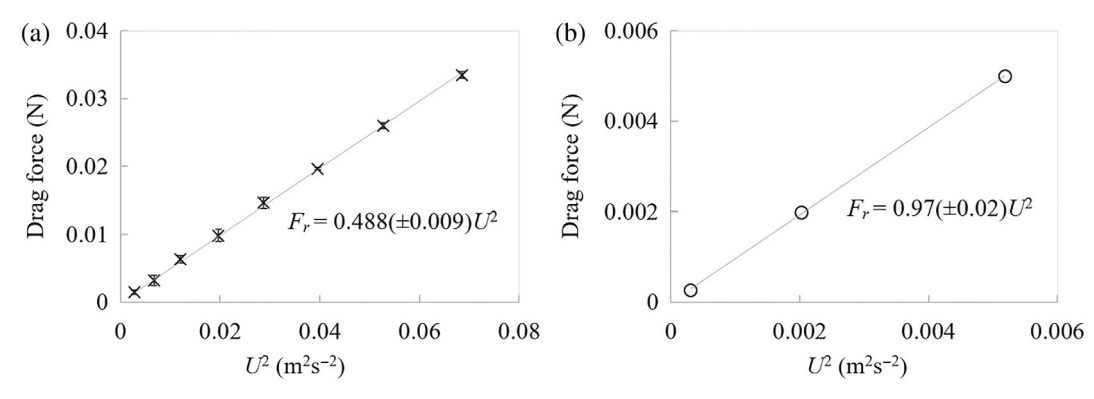


Fig. 7. Drag force vs. velocity squared for (a) the plastic plant with stem held rigidly with steel wire, and (b) the shortest *Bacopa caroliniana* at the lowest three velocities, for which minimal reconfiguration was observed, such that the drag is quadratic with the velocity over this range. The error bars are the standard deviation of four repeated force measurements.

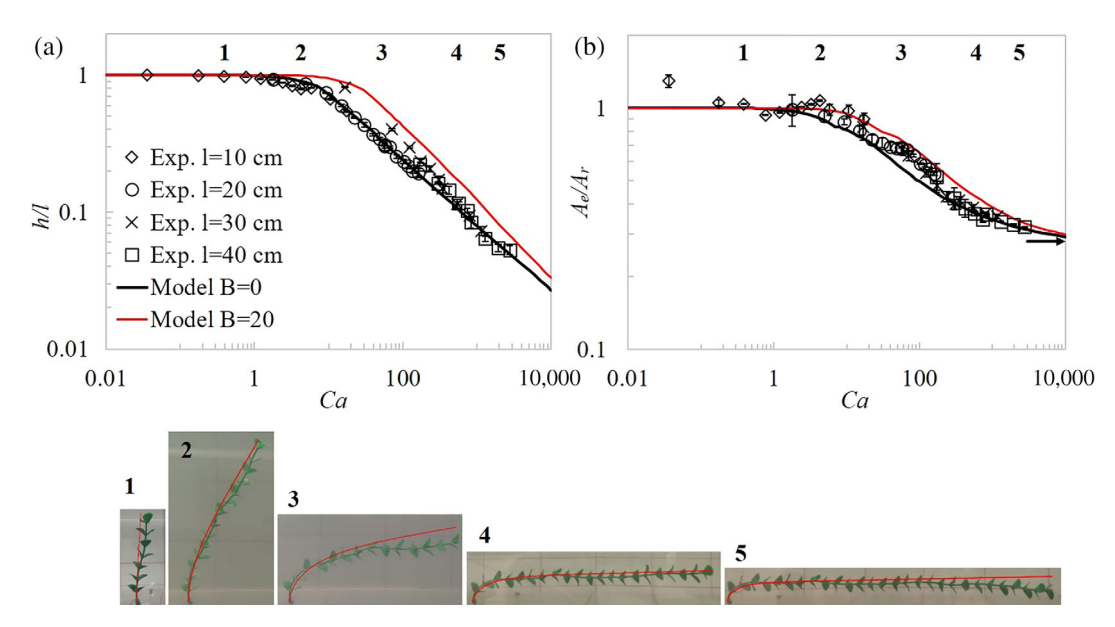


Fig. 8. (a) Normalized deflected height, h/l, vs. Cauchy number defined in Eq. 16. (b) Normalized effective frontal area, A_e/A_r , vs. Cauchy number. The symbols are measured values, and the lines are smoothed curves based on individual model predictions at 55 Cauchy numbers. The black arrow indicates the model predicted limiting value $A_e/A_r = 0.28$ from Eq. 12. The error bars indicate the standard deviation among four repeated measurements of force and 20 photos of postures for A_e/A_r and h/l, respectively. The bold numbers correspond to the images shown at the bottom, which correspond to Ca = 0.4, 5, 48, 540, and 1930. The red lines in the images are the model predicted postures.

 A_e/A_r were \pm 0.04 and \pm 0.1, respectively. The good agreement between prediction and measurement supported our assumptions, including the neglect of lift force. A negligible lift contribution may be attributed to the leaves being distributed in symmetric pairs (see Figs. 2, 3), so that the lift force on each leaf in a pair was roughly equal in magnitude but opposite in sign, such that the pair contributed negligible lift. However, we caution that this may not be true for all leaf morphology, because at large angles of attack the lift force is not necessarily symmetric. In addition, the influence of sheltering on the lift experienced by downstream leaves has not been defined and requires further study.

The ratio A_e/A_r exhibited four regions of behavior. First, for Ca < 1 the plant was not deflected (h/l = 1, Fig. 8a) and consistent with this A_e/A_r was close to 1 (Fig. 8b). For Ca = 1-10, the plant began to deflect (h/l < 1), but the drag ratio remained close to 1. In this range $\nu = -0.20 \pm 0.04$ ($A_e/A_r =$ $(1.02 \pm 0.03) Ca^{-0.10 \pm 0.02})$ and $\nu = -0.04 \pm 0.02$ $(A_e/A_r =$ $(1.01 \pm 0.02)Ca^{-0.02 \pm 0.01}$), based on the model prediction of B = 0 and B = 20, respectively. The Vogel number estimated from the measured drag fell in between these values, with $\nu = -0.06 \pm 0.04 \ (A_e/A_r = (1.0 \pm 0.1)Ca^{-0.03 \pm 0.02})$. The fact that drag remained high even as the plant deflected can be attributed to the leaves, which exhibit negligible reconfiguration. That is, for small stem deflections, the total area of leaves remained roughly constant, even as the projected areas of leaves on the upstream and downstream face of the stem changed. As the stem deflected, the angle between the leaves on the upstream face and the vertical first decreased until the leaves were in the vertical plane and then increased,

such that the projected leaf area initially increased and then decreased. However, the projected area of the leaves on the downstream side of the stem first decreased until the leaves were in the horizontal plane and then increased. These competing trends resulted in little change in total frontal area when the deflection was small (image 1 and image 2 in Fig. 8). In addition, at small stem deflection leaf sheltering was not important.

For 10 < Ca < 1000, the deflected plant height decreased rapidly with the increasing Ca (image 3 and image 4 in Fig. 8). Over this range of deflection, sheltering became increasingly important. The sheltering was predicted to begin at $h_c/l = 0.91$ (Table 1), which occurred at Ca = 5. For Ca = 10-1000, the Vogel number was $\nu = -0.46 \pm 0.04$ $(A_e/A_r = (1.6 \pm 0.1)$ $Ca^{-0.23 \pm 0.02}$, based on the measurements). This transition from a weaker to a stronger dependence on Ca (from $\nu = -0.06$ for 1 < Ca < 10 to $\nu = -0.46$ for 10 < Ca < 1000) was also presented in Figure 4b in Harder et al. (2004). Note that the peak magnitude of $\nu = -0.46$ was smaller than the value for simple 2-D bending ($\nu = -2/3$) (Alben et al. 2002; Gosselin et al. 2010; Gosselin and De Langre 2011; Luhar and Nepf 2011) and 3-D bending ($\nu = -4/3$) of simple structures (Gosselin et al. 2010), and this difference likely reflects the role of the leaves.

Finally, for Ca > 1000 (Fig. 8 image 5), the plant posture was horizontal, such that the sheltering coefficient C_s approached its limiting value C_{s0} . For perfectly horizontal stem posture, the model predicted a limiting value of $A_e/A_r = 0.25 \frac{|cos(\pi/2 - \alpha)| + |cos(\pi/2 + \alpha)|}{2|cos\alpha|} = 0.25 tan 48^{\circ} \approx 0.28$ (Eq. 13,

shown with a horizontal arrow in Fig. 8b). A limiting value of finite magnitude is not predicted by the previous 2-D and 3-D scaling laws, but it is likely an important aspect in all real plant morphology.

Reconfiguration of and drag on live plant B. caroliniana

The predictions of plant posture (h/l) and drag were also validated with live samples of B. caroliniana (Fig. 9), for which $\alpha = 112^{\circ}$, $h_c/l = 0.99$, and $C_{s0} = 0.125$ (Table 1). The plant remained upright when Ca < 1. For Ca > 1, the deflection was dependent on plant buoyancy, which was higher for the longer plant samples. Plant buoyancy has been observed to delay the reconfiguration of a single blade until $Ca^* > B$ (see discussion in Luhar and Nepf 2011). A similar tendency was seen here. Specifically, for the shorter plants with l = 9 cm and 17 cm, B = 1.4 and 8.6, respectively, and the strong reconfiguration (rapidly declining h/l in Fig. 9a) was delayed to Ca > 5. For the longer plant (l = 28 cm), B = 37, and the strong reconfiguration was delayeduntil Ca > 20. Importantly, at the start of plant reconfiguration, the reconfiguration was accompanied by an increase in drag (see Ca = 5-100 in Fig. 9b), and this behavior was captured by the model prediction (Fig. 9b). The greatest increase in drag (effective area) was 29% for both the measured and predicted results. This phenomenon has also been observed for tree branches (Vogel 1984) and a poroelastic ball (Gosselin and De Langre 2011). The magnitude of drag increase in our study was comparable to that of the poroelastic ball (18%, Figure 9 in Gosselin and De Langre 2011). The new model can explain this unusual trend. The B. caroliniana used in our experiment had a large leaf angle ($\alpha = 112^{\circ}$), so that the angle between the leaves

and the flow was small when stem deflection was small (see image 1 in Fig. 9). For small stem reconfiguration, the angle between the leaves and incoming flow initially increased, producing a larger projected area and hence a larger drag force. Note that leaf sheltering was not significant at these low Cauchy numbers, because the plant deflected height was higher than or close to the critical plant deflected height ($h_c = 0.99$) at which sheltering began. A similar progression can be described for the poroelastic ball. With the introduction of flow, filaments that initially point upstream become more perpendicular to the flow, with an associated increase in drag, but as velocity (Cauchy number) increases further, these filaments eventually bend downstream, with an associated decrease in drag (Gosselin and De Langre 2011).

Three images are shown at the bottom of Fig. 9 corresponding to the posture of the plant at Ca = 1, 80, and 2900. At the maximum Cauchy number 2900, the plant was almost horizontal, and A_e/A_r approached the model predicted limit $A_e/A_r = 0.31$ (estimated by Eq. 13 with $\theta = \pi/2$ and shown with the black arrow in Fig. 9b). At this high Cauchy number, slight vibration in the leaves and stem were observed. However, the leaves exhibited very little deformation, even at high Cauchy number, consistent with the model assumptions. The red lines indicate the predicted stem postures and illustrate a reasonable agreement between the observed and modeled postures. The maximum deviations between model and measurements in h/l and A_e/A_r are ± 0.12 and ± 0.2 , respectively. Over all, the model made a quite good prediction in both plant deflection and drag force reduction considering the complexity of the real plant morphology.

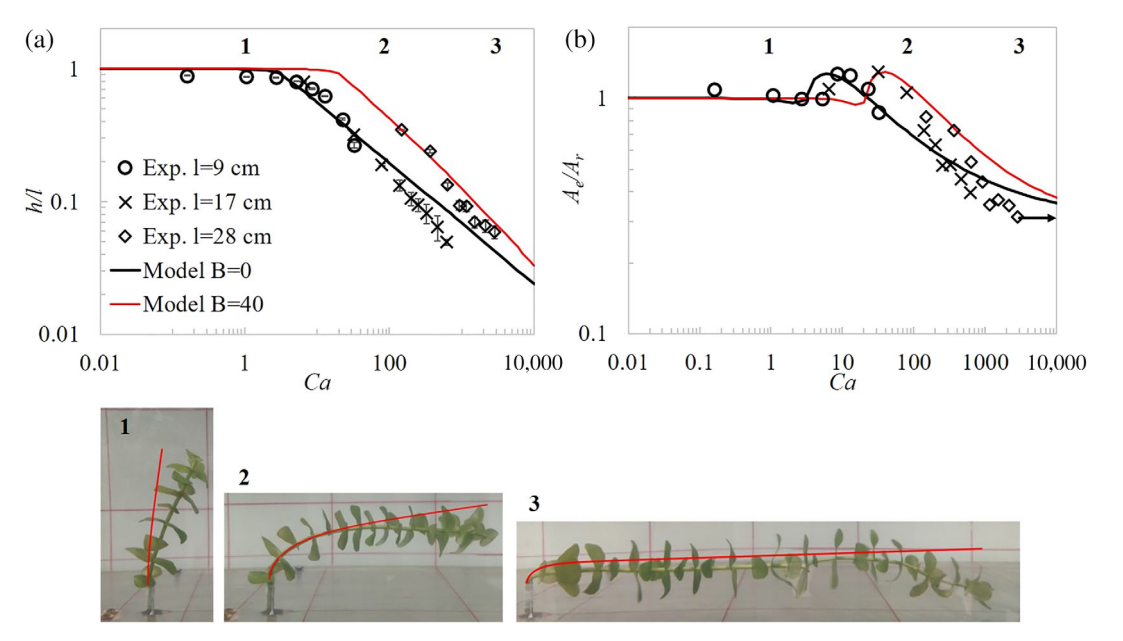


Fig. 9. Experiment and model prediction of (a) h/l and (b) A_d/A_r vs. Cauchy number. The symbols are measured values, and the lines are smoothed curves based on individual model predictions at 57 Cauchy numbers. The black arrow indicates the model predicted limiting value $A_d/A_r = 0.31$ from Eq. 12. The subplots labeled 1, 2, and 3 correspond to Cauchy number 1, 80, and 2900, respectively. The red curves in posture images are the model predicted postures.

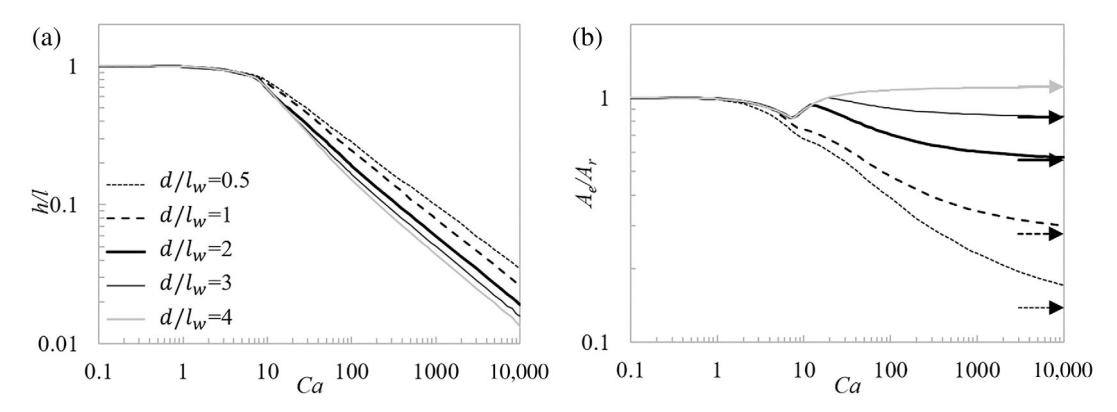


Fig. 10. Model predictions with constant leaf angle ($\alpha = 48^{\circ}$) and varied leaf spacing (d/l_w). (a) Deflected height, h, normalized by stem length, l, and (b) effective frontal area normalized by rigid plant frontal area vs. Cauchy number defined in Eq. 10. Buoyancy number B = 0. Horizontal arrows point to the limiting value of A_e/A_r predicted by Eq. (12) with $\theta = \pi/2$.

Discussion

The sheltering effect on drag reduction

This study developed a new sheltering-reconfiguration model, which was validated with measurements of both plastic R. bonsai and live B. caroliniana. The model can be used to explore how different plant structure, specifically, leaf spacing d, leaf width l_w , and leaf angle α , affect sheltering and impact drag. To focus on the influence of sheltering, the plant material density was assumed to be comparable to water so that B=0. Several species of live plant can be represented by the model, which assumes a single flexible stem and multiple leaves distributed along the stem, with leaves that undergo negligible reconfiguration (Table 2). For real plants, the leaf angle α ranges from 30° to 110°, and the ratio of leaf spacing to leaf width d/l_w ranges from 0.5 to 3.5 (estimated from web images of live plant with the links given in Table A1.).

First, the impact of leaf spacing on stem deflection and drag was studied with d/l_w = 0.5, 1, 2, 3, and 4 at a fixed leaf angle

 $\alpha=48^\circ$ (the same as *R. bonsai*). Second, the impact of leaf angle on stem deflection and drag was considered for $d/l_w=1$ and for a range of leaf angles, summarized in Table 3. Note that $A_l \mid cos(\pi-\alpha) \mid = A_l \mid cos(\alpha) \mid$, such that $90^\circ < \alpha < 180^\circ$ has the same result as $\pi-\alpha$. For each model run, Eqs. 13, 14, and 15 were used to define the limiting sheltering coefficient, C_{s0} , and the corresponding equation of C_s for each plant model, and these are listed in Table 3.

With a constant leaf angle ($\alpha=48^{\circ}$), variation in leaf spacing had little impact on the plant posture (Fig. 10a), but a significant impact on plant drag (Fig. 10b). The horizontal arrows at the right hand axis of Fig. 10b indicate the minimum values of A_e/A_r , which were calculated by Eq. 13 with $\theta=\pi/2$, i.e., with horizontal stem posture. In each case, the effective frontal area approached the minimum value between Ca=1000 and 10,000. At the point of maximum stem deflection, leaf sheltering produced a great variation in effective frontal area, spanning $A_e/A_r=1.1$ for leaf spacing $d/l_w=4$ with

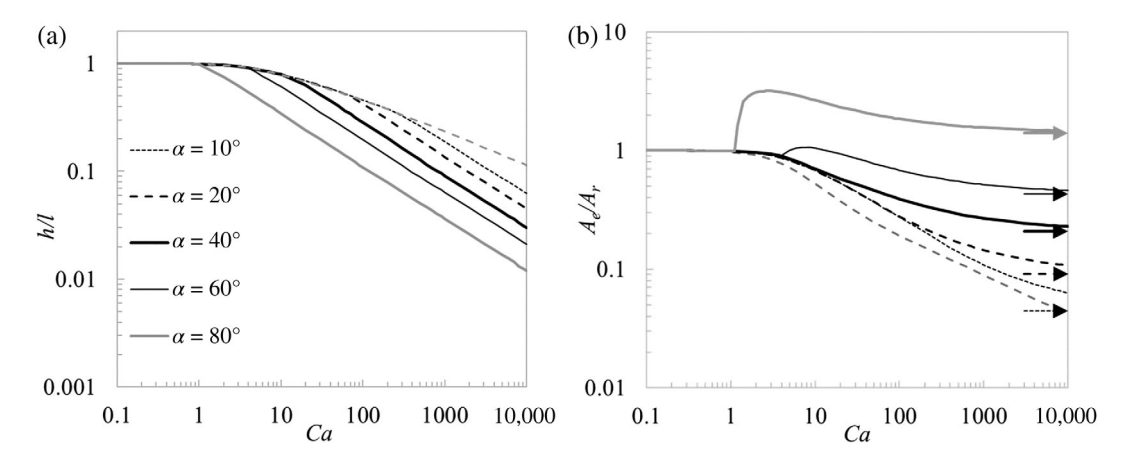


Fig. 11. Model predictions with leaf spacing $(d/l_w = 1)$ and varied leaf angle (α) . (a) Deflected height, h, normalized by stem length, l, and (b) effective frontal area normalized by rigid plant frontal area, as a function of Cauchy number, defined in Eq. 10. Buoyancy number is set to 0. Horizontal arrows point to the limiting value of A_e/A_r predicted by Eq. 12 with $\theta = \pi/2$. The dashed gray curves indicate the reconfiguration of and drag on a single flat blade with no leaves, described in Luhar and Nepf (2011).

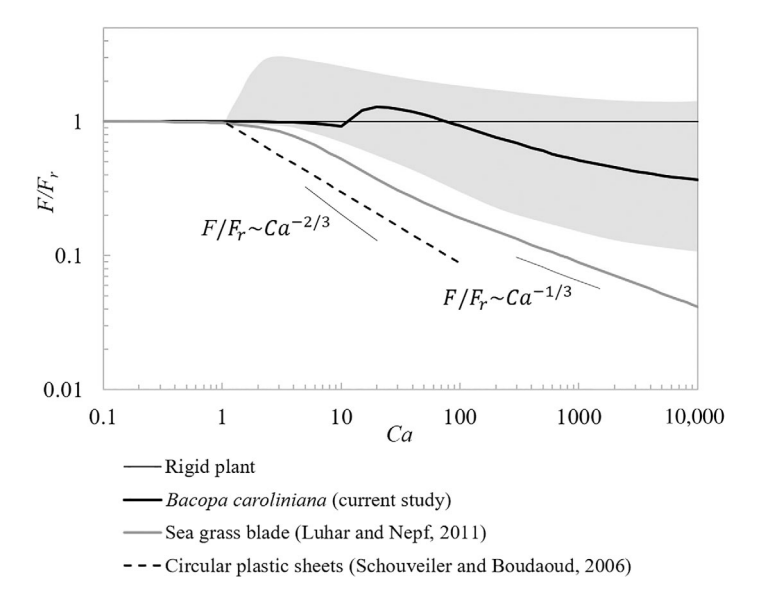


Fig. 12. The drag on a flexible plant, F_r , normalized by the drag on a rigid plant with the same morphology, F_r , as a function of Cauchy number for (1) a rigid plant with no reconfiguration (black line), (2) a seagrass blade exhibiting 2-D reconfiguration (gray curve based on Luhar and Nepf 2011, with B=0), (3) a flat disk rolling up, representing 3-D reconfiguration (dash line based on Fig. 6 [triangle] in Schouveiler and Boudaoud 2006, and (4) *Bacopa caroliniana* with stem reconfiguration and leaf sheltering (thick black curve, with B=40). The gray region span the drag behavior over the parameter range $\alpha=20^\circ-80^\circ$ and $d/l_w=0.5-2$, based on Table 3 and model results shown in Figs. 10, 11.

no sheltering to $A_e/A_r = 0.14$ for leaf spacing $d/l_w = 0.5$. Note that for the leaf spacing $d/l_w = 4$, the drag increased with increased stem reconfiguration, which reflected the absence of leaf sheltering. This trend has not been previously reported. Also note that none of the plants listed in Table 2 exhibit this spacing. Most plants have leaf spacing 0.5–2, for which leaf sheltering contributes to a reduction in drag (A_e/A_r) during reconfiguration (Fig. 10b). Therefore, the

model results suggest that the commonly observed leaf spacing (Table 2) is selected because it facilitates leaf sheltering. However, as shown in the next example, for larger leaf angles, enhanced drag with reconfiguration can occur for smaller spacing between leaves.

For a constant leaf spacing $(d/l_w = 1)$, variation in leaf angle, α , impacted the Cauchy number dependence of both deflected height and drag (Fig. 11). For small Ca, the stem deflected height followed the same dependence observed for a stem without leaves (represented by the 2-D bending model shown with the dashed gray line in Fig. 11a). However, at higher Cauchy number the stem with leaves pronated more rapidly (smaller h/I) than the stem without leaves, and the deviation from simple 2-D bending (dashed curve) occurred sooner (at smaller Ca) for greater leaf angle. After deviating from the 2-D bending curve, the plants with leaves all followed the same dependence, $h/l\sim Ca^{-0.48\pm0.01}$ (Fig. 11a). Despite the similar scale dependence observed in stem deflection, the variation in drag force with Ca exhibited great variation with the leaf angle α (Fig. 11b). As expected, for $Ca \le 1$, the plant did not deflect (h/l = 1) and $A_e/A_r = 1$. For 1 < Ca < 10, drag force increased for $\alpha = 60^{\circ}$ and 80° , but decreased for all smaller angles. For example, when $\alpha = 80^{\circ}$ and Ca = 2, the drag force increased to three times the drag generated by a rigid plant. For 10 < Ca < 1000, drag declined with increasing Ca for all leaf angles, but the rate of decline increased with decreasing α . and the greatest decrease occurred for $\alpha = 10^{\circ}$. For Ca > 1000, A_e/A_r approached the limiting value for horizontal posture, indicated with horizontal arrows, and this minimum drag decreased with decreasing leaf angle.

A range of drag reduction for flexible plants

The way that reconfiguration impacts drag varies with plant morphology and rigidity. The range of behavior is illustrated in Fig. 12, which shows the ratio of drag on a flexible plant, *F*, normalized by the drag on a rigid plant of the same

Table 2. List of plants with distributed leaves along a single stem, with leaf angle, α , and the ratio of leaf spacing to leaf width, d/l_w . Values of α and d/l_w were estimated from images of live plants with uncertainty \pm 15° in α and \pm 0.2 in d/l_w . The images, except *B. caroliniana* and *R. bonsai*, were found on webpages given in Table A1.

Species	α	d/I_w	Species	α	d/I_w
Bacopa araguaia	55°	1.4	Micranthemum umbrosum	72°	1.6
Bacopa caroliniana	112°	0.5	Nesaea icosandra	70°	1.3
Bacopa colorata	73°	0.5	Nesaea triflora	37°	2.3
Bacopa salzmannii	86°	1.3	Oldenlandia salzmannii	86°	1.3
Bacopa monnieri	94°	1.4	Rotala bonsai	48°	1.0
Cuphea anagalloidea	57°	1.4	Rotala indica	52°	0.7
Elatine orientaris	64°	1.5	Rotala macrandra	66°	0.9
Hedyotis salzmannii	39°	1.4	Rotala macrandra "green"	52°	0.6
Limnophila fragrans	68°	1.8	Rotala macrandra variegata	84°	0.8
Lindernia grandiflora	34°	0.5	Rotala sp. "indian"	71°	1.0
Lindernia parviflora	84°	1.7	Rotala sp. "mini type 1"	105°	0.7

Table 3. Model parameters used to explore the influence of (a) varied leaf spacing with leaf angle held constant at $\alpha = 48^{\circ}$ and (b) varied leaf spacing with leaf angle held constant at $\alpha = 48^{\circ}$ and (b) varied leaf spacing with leaf angle held constant at $\alpha = 48^{\circ}$ and (b) varied leaf spacing with leaf angle held constant at $\alpha = 48^{\circ}$ and (b) varied leaf spacing with leaf angle held constant at $\alpha = 48^{\circ}$ and (b) varied leaf spacing with leaf angle held constant at $\alpha = 48^{\circ}$ and (b) varied leaf spacing with leaf angle held constant at $\alpha = 48^{\circ}$ and (b) varied leaf spacing with leaf angle held constant at $\alpha = 48^{\circ}$ and (b) varied leaf spacing with leaf angle held constant at $\alpha = 48^{\circ}$ and (b) varied leaf spacing with leaf angle held constant at $\alpha = 48^{\circ}$ and (b) varied leaf space with leaf angle held constant at $\alpha = 48^{\circ}$ and (b) varied leaf space with leaf space with leaf angle held constant at $\alpha = 48^{\circ}$ and (b) varied leaf space with leaf space with leaf angle held constant at $\alpha = 48^{\circ}$ and (b) varied leaf space with leaf spac
ied leaf angle with leaf spacing held constant at $d/l_w = 1$. Eqs 13, 14, and 15 were used to define h_c , C_{s0} , and C_s .

(a) Leaf angle $\alpha = 48^{\circ}$			(b) Leaf spacing $d/I_w = 1$				
d/I_w	h _c /I	C_{s0}	$C_s(h < h_c)$	α	h _c /I	C_{s0}	$C_s(h < h_c)$
0.5	1	0.125	$0.875\frac{h}{l} + 0.125$	10°	0.996	0.25	$0.753\frac{h}{l} + 0.25$
1	0.914	0.25	$0.821\frac{h}{l} + 0.25$	20°	0.985	0.25	$0.762\frac{h}{l} + 0.25$
2	0.595	0.5	$0.840\frac{h}{l} + 0.5$	40°	0.940	0.25	$0.798\frac{h}{l} + 0.25$
3	0.444	0.75	$0.564\frac{h}{l} + 0.75$	60°	0.866	0.25	$0.866 \frac{h}{l} + 0.25$
4	0.348	1	1	80°	0.892	0.25	$0.841\frac{h}{l} + 0.25$

morphology, F_r . Rigid plants, such as mangrove roots and tree trunks, do not reconfigure and follow the quadratic drag law, such that $F/F_r = 1$ (black line in Fig. 12). A seagrass blade or simple cylindrical stem exhibits 2-D reconfiguration, follows the scaling $F/F_r \sim Ca^{-1/3}$ ($\nu = -2/3$) for Ca > 10 (gray curve in 12). A circular plastic sheet (Schouveiler and Boudaoud 2006), representative of some leaves, reconfigures in both the lateral and vertical dimensions, and follows the scaling for 3-D reconfiguration, $F/F_r \sim Ca^{-2/3}$, $\nu = -4/3$ (Schouveiler and Boudaoud 2006; Gosselin et al. 2010; Gosselin 2019) for Ca > 1 (dashed line in Fig. 12). Finally, plants with multiple leaves distributed along a flexible stem (Table 2) are influenced by both stem reconfiguration and leaf sheltering. For these plants, the dependence of drag on Cauchy number depends on plant structure, and in particular on the ratio of leaf spacing to leaf width, d/l_w , and leaf angle, α . For example, when B. caroliniana $(d/l_w = 0.5, \alpha = 112^\circ)$ begins to reconfigure, the drag force increases over the range 1 < Ca < 30, and then decreases for Ca > 30 following F/ $F_r \sim Ca^{-0.22}$ ($\nu = -0.44$) (thick black curve in Fig. 12). As listed in Table 2, leaf spacing most commonly falls between $d/l_w = 0.5$ and 2 and leaf angle between $\alpha = 20^{\circ}$ and 80° , for which the model developed in this paper predicts a wide range of force variation with Ca, represented by the light gray shading

Previous studies have considered Cauchy numbers up to the order of 1000, and focused on the trend of decreasing drag with increasing reconfiguration (Gosselin and De Langre 2011; Luhar and Nepf 2011; Li et al. 2018). However, the present study has highlighted that there is a limit in drag reduction, and the necessarily existence of a maximum deflection with a finite, minimum drag (e.g., Figs 3, 8). Luhar and Nepf (2011) noted that even as the form drag on a seagrass blade decreases with reconfiguration, the frictional drag will eventually become important when the majority of the blade is aligned with the flow. Figure 5 in Gosselin et al. 2010 also shows that the drag on a flexible plate tends away from the -4/3 slope and levels off to a constant for Cauchy greater than 1000. The existence of a finite minimum drag is important to consider when modeling real vegetated systems.

Conclusion

This paper extended previous models (Gosselin et al. 2010; Gosselin and De Langre 2011; Luhar and Nepf 2011) describing the impact of plant reconfiguration on plant drag by considering the more complex morphology of a flexible stem with multiple leaves. The new model considered the sheltering between leaves using a sheltering coefficient, C_s (Eq. 15). The new model was validated by successfully predicting the reconfiguration and drag for the live plant B. caroliniana. The sheltering of leaves provided an additional mechanism through which drag can be reduced during plant reconfiguration. The impact of sheltering was shown to depend on leaf size, spacing, angle of leaf to the stem, and the stem deflection. Importantly, a new regime was revealed for leaves attached to the stem at an angle close to 90°, in which the drag increased for an initial degree of stem reconfiguration, before subsequently decreasing with greater reconfiguration. In addition, new observations and modeling illustrated the existence of a finite minimum drag, which occurs when the stem reaches a horizontal posture, and which must be considered to properly represent real vegetation. This limit was not predicted by previous models.

References

Alben, S., M. Shelley, and J. Zhang. 2002. Drag reduction through self-similar bending of a flexible body. Nature **420**: 479–481. doi:10.1038/nature01232

Arkema, K. K., R. Griffin, S. Maldonado, J. Silver, J. Suckale, and A. D. Guerry. 2017. Linking social, ecological, and physical science to advance natural and nature-based protection for coastal communities: Advancing protection for coastal communities. Ann. N.Y. Acad. Sci. **1399**: 5–26. doi: 10.1111/nyas.13322

Barbier, E. B., S. D. Hacker, C. Kennedy, E. W. Koch, A. C. Stier, and B. R. Silliman. 2011. The value of estuarine and coastal ecosystem services. Ecol. Monogr. **81**: 169–193. doi: 10.1890/10-1510.1

Barsu, S., D. Doppler, J. J. S. Jerome, N. Rivière, and M. Lance. 2016. Drag measurements in laterally confined 2D

- canopies: Reconfiguration and sheltering effect. Phys. Fluids **28**: 107101. doi:10.1063/1.4962309
- Bitsuamlak, G. T., A. K. Dagnew, and J. Erwin. 2010. Evaluation of wind loads on solar panel modules using CFD. *The Fifth International Symposium on Computational Wind Engineering*. Proceedings of the CWE2010.
- Blevins, R. D. B. 1979. Formulas for natural frequency and mode shape. Van Nostrand Reinhold Company.
- Blevins, R. D. B. 1990. Flow-induced vibration, 2nd ed. Florida, USA: Krieger Publishing.
- Carrington, E. 1990. Drag and dislodgment of an intertidal macroalga: Consequences of morphological variation in mastocarpus papillatus kützing. J. Exp. Mar. Biol. Ecol. **139**: 185–200. doi:10.1016/0022-0981(90)90146-4
- Costanza, R., R. d'Arge, R. de Groot, et al. 1997. The value of the world's ecosystem services and natural capital. Nature. **387**(6630): 253–260.
- de Langre, E., A. Gutierrez, and J. Cossé. 2012. On the scaling of drag reduction by reconfiguration in plants. Compt. Rend. Mécan. **340**: 35–40. doi:10.1016/j.crme.2011.11.005
- Duan, J. G., B. Barkdoll, and R. French. 2006. Lodging velocity for an emergent aquatic plant in open channels. J. Hydraul. Eng. **132**: 1015–1020. doi:10.1061/!ASCE"0733-9429! 2006"132:10!1015"
- Friedland, M. T., and M. W. Denny. 1995. Surviving hydrodynamic forces in a wave-swept environment: Consequences of morphology in the feather boa kelp, *Egregia menziesii* (turner). J. Exp. Mar. Biol. Ecol. **190**: 109–133. doi:10.1016/0022-0981(95)00038-S
- Gaylord, B., C. A. Blanchette, and M. W. Denny. 1994. Mechanical consequences of size in wave-swept algae. Ecol. Monogr. **64**: 287–313. doi:10.2307/2937164
- Gillies, J. A., W. G. Nickling, and J. King. 2002. Drag coefficient and plant form response to wind speed in three plant species: Burning Bush (*Euonymus alatus*), Colorado Blue Spruce (*Picea pungens* glauca.), and Fountain Grass (*Pennisetum setaceum*). J. Geophys. Res. **107**: 4760. doi:10. 1029/2001JD001259
- Goring, D. G., and V. I. Nikora. 2002. Despiking acoustic Doppler velocimeter data. J. Hydraul. Eng. **128**: 117–126. doi:10.1061/(ASCE)0733-9429(2002)128:1(117)
- Gosselin, F. P. 2019. Mechanics of a plant in fluid flow. J. Exp. Bot. **70**: 3533–3548. doi:10.1093/jxb/erz288
- Gosselin, F., E. de Langre, and B. A. Machado-Almeida. 2010. Drag reduction of flexible plates by reconfiguration. J. Fluid Mech. **650**: 319–341. doi:10.1017/S0022112009993673
- Gosselin, F. P., and E. de Langre. 2011. Drag reduction by reconfiguration of a poroelastic system. J. Fluids Struct. **27**: 1111–1123. doi:10.1016/j.jfluidstructs.2011.05.007
- Greiner, J. T., K. J. McGlathery, J. Gunnell, and B. A. McKee. 2013. Seagrass restoration enhances "blue carbon" sequestration in coastal waters J. Cebrian [ed.]. PLoS One 8: e72469. doi:10.1371/journal.pone.0072469

- Harder, D. L., O. Speck, C. L. Hurd, and T. Speck. 2004. Reconfiguration as a prerequisite for survival in highly unstable flow-dominated habitats. J. Plant Growth Regul. **23**: 98–107. doi:10.1007/s00344-004-0043-1
- Hassani, M., N. W. Mureithi, and F. P. Gosselin. 2016. Large coupled bending and torsional deformation of an elastic rod subjected to fluid flow. J. Fluids Struct. **62**: 367–383. doi:10.1016/j.jfluidstructs.2015.12.009
- Jalonen, J., and J. Järvelä. 2013. Impact of tree scale on drag: Experiments in a towing tank. *Proceedings of 2013 IAHE World Congress*.
- Jin, Y., J. T. Kim, Z. Mao, and L. P. Chamorro. 2018. On the couple dynamics of wall-mounted flexible plates in tandem. J. Fluid Mech. **852**: 852. doi:10.1017/jfm.2018.580
- Lei, J., and H. Nepf. 2019. Blade dynamics in combined waves and current. J. Fluids Struct. **87**: 137–149. doi:10.1016/j. jfluidstructs.2019.03.020
- Li, Y. H., L. Xie, and T. C. Su. 2018. Resistance of openchannel flow under the effect of bending deformation of submerged flexible vegetation. J. Hydraul. Eng. **144**: 04017072. doi:10.1061/(ASCE)HY.1943-7900.0001419
- Luhar, M., and H. M. Nepf. 2011. Flow-induced reconfiguration of buoyant and flexible aquatic vegetation. Limnol. Oceanogr. **56**: 2003–2017. doi:10.4319/lo.2011.56.6.2003
- Luhar, M., and H. M. Nepf. 2013. From the blade scale to the reach scale: A characterization of aquatic vegetative drag. Adv. Water Resour. **51**: 305–316. doi:10.1016/j.advwatres. 2012.02.002
- Nikora, V., and D. Goring. 2000. Flow turbulence over fixed and weakly mobile gravel beds. J. Hydraul. Eng. **126**: 679–690. doi:10.1061/(ASCE)0733-9429(2000)126:9(679)
- Pan, Y., E. Follett, M. Chamecki, and H. Nepf. 2014. Strong and weak, unsteady reconfiguration and its impact on turbulence structure within plant canopies. Phys. Fluids **26**: 105102. doi:10.1063/1.4898395
- Puijalon, S., G. Bornette, and P. Sagnes. 2005. Adaptations to increasing hydraulic stress: Morphology, hydrodynamics and fitness of two higher aquatic plant species. J. Exp. Bot. **56**: 777–786. doi:10.1093/jxb/eri063
- Sand-Jensen, K. 2003. Drag and reconfiguration of freshwater macrophytes. Freshw. Biol. **48**: 271–283. doi:10.1046/j. 1365-2427.2003.00998.x
- Schouveiler, L., and A. Boudaoud. 2006. The rolling up of sheets in a steady flow. J. Fluid Mech. **563**: 71. doi:10. 1017/S0022112006000851
- Schutten, J., and A. J. Davy. 2000. Predicting the hydraulic forces on submerged macrophytes from current velocity, biomass and morphology. Oecologia **123**: 445–452. doi:10. 1007/s004420000348
- Schutten, J., J. Dainty, and A. J. Davy. 2005. Root anchorage and its significance for submerged plants in shallow lakes. J. Ecol. **93**: 556–571. doi:10.1111/j.1365-2745.2005. 00980.x

- Tang, J., S. Ye, X. Chen, H. Yang, X. Sun, F. Wang, Q. Wen, and S. Chen. 2018. Coastal blue carbon: Concept, study method, and the application to ecological restoration. Sci. China Earth Sci. 61: 637–646. doi:10.1007/s11430-017-9181-x
- Usherwood, J. R., A. R. Ennos, and D. J. Ball. 1997. Mechanical and anatomical adaptations in terrestrial and aquatic buttercups to their respective environments. J. Exp. Bot. **48**: 1469–1475. doi:10.1093/jxb/48.7.1469
- Västilä, K., and J. Järvelä. 2014. Modeling the flow resistance of woody vegetation using physically based properties of the foliage and stem. Water Resour. Res. **50**: 229–245. doi: 10.1002/2013WR013819
- Vogel, S. 1984. Drag and flexibility in sessile organisms. Am. Zool. **24**: 37–44. doi:10.1093/icb/24.1.37
- Vogel, S. 1989. Drag and reconfiguration of broad leaves in high winds. J. Exp. Bot. **40**: 941–948. doi:10.1093/jxb/40. 8.941
- Wang, H., and E. S. Takle. 1997. Momentum budget and shelter mechanism of boundary-layer flow near a shelterbelt. Bound.-Lay. Meteorol. **82**: 417–437. doi:10.1023/A: 1000262020253
- Waycott, M., B. J. Longstaff, and J. Mellors. 2005. Seagrass population dynamics and water quality in the great barrier reef region: A review and future research directions. Mar. Pollut. Bull. **51**: 343–350. doi:10.1016/j.marpolbul.2005. 01.017
- Whittaker, P., C. Wilson, J. Aberle, H. P. Rauch, and P. Xavier. 2013. A drag force model to incorporate the reconfiguration

- of full-scale riparian trees under hydrodynamic loading. J. Hydraul. Res. **51**: 569–580. doi:10.1080/00221686.2013. 822936
- Wu, Z., B. Gong, Z. Wang, Z. Li, and C. Zang. 2010. An experimental and numerical study of the gap effect on wind load on heliostat. Renew. Energy **35**: 797–806. doi:10.1016/j. renene.2009.09.009
- Xavier, P., C. Wilson, J. Aberle, H. P. Rauch, W. Lammeranner, and H. Thomas. 2010. Drag force of flexible submerged trees. *Proceedings of the HYDRALAB III Joint User Meeting*.

Acknowledgments

We thank Dr. Jiarui Lei for his guidance with the experimental equipment. Xiaoxia Zhang was supported by the China Scholarship Council (CSC) and the Ministry of Science and Technology of the People's Republic of China (MST) under the High-level Overseas Talents introducing project (No. G20190023062). The project also received support from the US National Science Foundation under EAR 1659923. Any opinions and conclusions are those of author(s) and do not necessarily reflect the views of C. S. C., M. S. T., or N. S. F.

Conflict of Interest

None declared.

Submitted 03 December 2019 Revised 26 March 2020 Accepted 21 May 2020

Associate editor: Julia Mullarney

Appendix A.

Table A1. List of links of webpage photos used to estimate α and d/l_w

Name	Link			
Bacopa araguaia	http://shuicao.cc/baike/view-1821.html			
Bacopa colorata	http://202.39.251.199/encyclopaedia/plant?plantID=207			
Bacopa salzmannii	http://202.39.251.199/encyclopaedia/plant?plantID=992			
Bacopa monnieri	http://shuicao.cc/baike/view-402.html			
Cuphea anagalloidea	http://www.denatuurinhuis.nl/zen/index.php?album=Plantenℑ=cuphea-anagalloidea.jpg			
Elatine orientaris	http://202.39.251.199/encyclopaedia/plant?plantID=343			
Hedyotis salzmannii	https://pearlingplants.com/products/hedyotis-salzmannii-live-aquarium-plants			
Limnophila fragrans	https://www.aquagreen.com.au/plant_data/Limnophila_fragrans.html			
Lindernia grandiflora	https://www.aquaticplantcentral.com/forumapc/plantfinder/details.php?id=340			
Lindernia parviflora	http://www.staraqua.ru/content/lindernia-parviflora-variegated			
Micranthemum umbrosum	https://aqualabaquaria.com/products/micranthemum-umbrosum			
Nesaea icosandra	http://202.39.251.199/encyclopaedia/plant?plantID=499			
Nesaea triflora	http://www.staraqua.ru/content/nesaea-triflora			
	http://202.39.251.199/encyclopaedia/plant?plantID=974			

(Continues)

Table A1. Continued

Name	Link
Oldenlandia salzmannii	
Rotala indica	http://shuicao.cc/baike/view-1881.html
Rotala macrandra	https://www.aquariumplantsfactory.com/products/rotala-macrandra?variant=28553780428861¤cy=USD&utm_campaign=gs-2018-12-09&utm_source=google&utm_medium=smart_campaign
Rotala macrandra "green"	http://202.39.251.199/encyclopaedia/plant?plantID=242
Rotala macrandra variegata	http://shuicao.cc/baike/view-1913.html
Rotala sp. "indian"	http://shuicao.cc/baike/view-3520.html
Rotala sp. "mini type 1"	http://202.39.251.199/encyclopaedia/plant?plantID=249